Investigating the effect of variable UAV altitude control on emitter localization

Marcel Kurz, Folker Hoffmann, André Brandenburger, Alexander Charlish
{marcel.kurz, folker.hoffmann, andre.brandenburger, alexander.charlish}@fkie.fraunhofer.de

***Abstract*—This research paper investigates the anticipated improvement in emitter localization time simulating a UAV (unmanned aerial vehicle) sensor platform that allows for variable flight altitudes, contrary to maintaining a fixed flight altitude. The study aims to quantify efficiency gain and evaluates whether these gains justify the additional hardware and software complexities involved with variable flight control. The considered UAV sensor platform carries a radio-frequency (RF) direction-finder system. The sensor platform is maneuvered by a controller maximizing the Fisher information to minimize the required mission time until emitter localization. Additionally, a benchmark control strategy further introduced as *Loitering* is considered, which steers the platform in a circular maneuver around the emitter at constant radius. Simulations are conducted involving various parameters to thoroughly compare the altitude control modes and quantifying the improvements of enabling *variable* altitude control. The comparison reveals only minor improvements in the scenarios, which initialize the sensor platform at altitudes lower than 50 [m]. The effort required to fulfil the requirements for *variable* height control is discussed, with the conclusion that the effort does not outweigh the effect for UAVs with initial altitudes below 50 [m].**

I. Introduction and Related Work

We consider the problem shown in figure 1 of localizing a stationary emitter with measurements acquired from a radio frequency (RF) direction-finder antenna that is mounted on a maneuverable UAV sensor platform. The RF antenna measurements only provide a bearing without range. Measurement noise is also considered to model the expected real-life behavior more closely. To determine the emitter location the platform must acquire measurements from multiple positions, due to unknown range from the emitter and the considered measurement noise. The path taken during the measurement process significantly influences the time required for localization. Comparative analysis of various path planning algorithms itself constitutes a broad field of research. These algorithms span from greedy planner in [1] and online optimization in [2] to those incorporating reinforcement learning techniques in [3]. The path planning algorithm applied in this paper utilizes the Fisher information matrix (FIM) about the estimated emitter location belief.

The FIM controller considred in this paper, produces a desired sensor platform position, that maximizes the information gain. Path planning for emitter localization that utilize the FIM has been considered intensively in [4]–[6]. Reduction of mission time by comparing different control approaches is studied in the works of [1], [7]: The time until localization was studied by [1] for a greedy planning algorithm and an

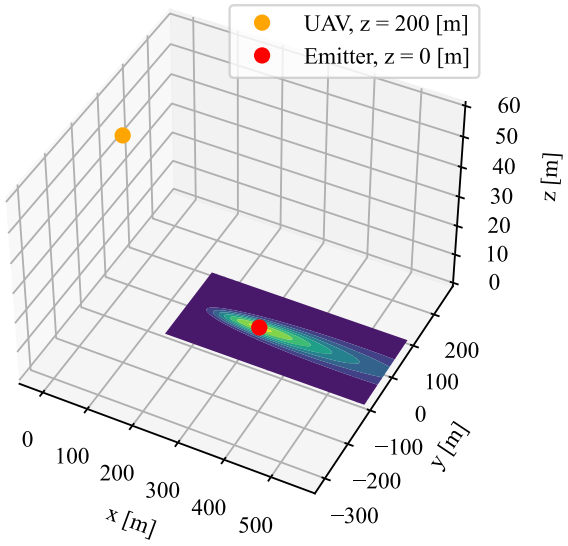

Fig. 1: The received bearing measurement is combined with the assumed standard deviation to form an area at the assumed altitude z = 0 [m] in which the emitter (red) is expected to be located. Maneuvering the UAV sensor platform (orange) provides additional measurements that are integrated into the belief about the emitter location. The goal of the UAV flight in this paper is to maneuver and thus reduce the expected area to the desired degree.

algorithm depending on the expected entropy by [8]. [9] utilized the Fisher information in a base policy for policy rollout action selection before the mission time is also compared towards an entropy-based planner. The mentioned works all contain the common simplification to constrain the path to a *fixed* altitude to perform planning in two dimensions. In [10] a FIM controller with both *variable* and *fixed* altitude is considered. [10] provides data that shows the same behaviour observed as in this paper: The time until localization is reduced for flights with *variable* altitude control. The existing works intensively compare *fixed* altitude controller with different control algorithms. The work by [10] does not quantify the observed improvement in the considered scenario between the *fixed* and the *variable* altitude controller. This paper fills this gap by quantifying how much faster an emitter is localized with a FIM controller when *variable* altitude control is enabled in comparison to a sensor platform constrained to a *fixed* altitude.

Enabling the option to switch on *variable* altitude control also introduces challenges besides the expected efficiency improvements. The platform requires a form of collision avoidance to not collide with 3D obstacles in the action space. Sometimes the altitude control is performed different within the control interface [11] leading to more complex code and therefore warranting more testing. Additional hardware requirements contradict the desired lightweight and cost-effective solutions applied in [1], [12]. Finally, it becomes more difficult to operate the platform in a crowded airspace as a simple separation by altitude becomes infeasible.

In this paper the margin of improvement is quantified, and it is discussed whether it is worth overcoming the challenges associated with enabling *variable* altitude control. A second perspective on the reduction of the mission time is provided by considering the *Loitering* controller [13] as an alternative control appraoch. The remaining part of this paper is structured as follows: The system model and the measurement function are described in section II. Followed by the required derivations for the FIM controller including the optimization problem formulation in section III. In section IV the considered simulation scenarios and sensor parameter are described, before in section IV the results are summarized. In section VI the results of the paper are concluded.

II. System Model

The system is modeled in a state space with the system equations

$$\mathbf{x}_{p,k+1} = \mathbf{x}_{p,k} + \mathbf{u}_k \tag{1}$$

$$\mathbf{x}_{p,k} = [x_{p,k}, y_{p,k}, z_{p,k}]^T \tag{2}$$

$$\mathbf{u}_k = \begin{bmatrix} \Delta x_{p,k} \\ \Delta y_{p,k} \\ \Delta z_{p,k} \end{bmatrix} = \begin{bmatrix} x_{sp,k} - x_{p,k} \\ y_{sp,k} - y_{p,k} \\ z_{sp,k} - z_{p,k} \end{bmatrix} \tag{3}$$

with the system state $\mathbf{x}_{p,k}$ and the control input u_k. The system state $\mathbf{x}_{p,k}$ contains the platform coordinates $[x_{p,k}, y_{p,k}, z_{p,k}]^T$. The platforms yaw, pitch and roll orientation are disregarded in this approach because it is assumed that the internal controller of the platform levels the platform in every timestep. The emitter location is denoted as $\mathbf{x}_{e,k} = [x_{e,k}, y_{e,k}, z_{e,k}]^T$. The emitter altitude is assumed to be known at ground level $z_{e,k} = 0$. The distance between the platform and the emitter is denoted as $r = ||\mathbf{x}_{e,k} - \mathbf{x}_{p,k}||_2$. The measurements are modeled as bearings towards a stationary emitter.

$$\begin{aligned} \mathbf{z}_k &= \begin{bmatrix} h_{az}(\Delta x_k, \Delta y_k) \\ h_{el}(\Delta x_k, \Delta y_k) \end{bmatrix} \\ &= \begin{bmatrix} \arctan 2(\Delta y_k, \Delta x_k) - \alpha_p \\ \arcsin(\Delta z_k / r_k) \end{bmatrix} + \omega \,, \end{aligned} \tag{4}$$

where the platform yaw angle α_p is assumed to be always known and thus can be neglected. The measurement noises are assumed to be Gaussian distributed with $\omega \sim \mathcal{N}(\mathbf{0}, \mathbf{R})$ and

$$\mathbf{R} = \begin{bmatrix} (\sigma_{az})^2 & 0 \\ 0 & (\sigma_{el})^2 \end{bmatrix} \tag{5}$$

The measurement noise leads to different area of confidence around the expected emitter location as depicted in 2. Measuring the bearing towards the ground-level emitter from an UAV at z = 200 [m] results in a smaller cross-sectional area compared to the area resulting from the UAV at z = 50 [m]. This consideration leads to the expectation that a change in altitude will have a measurable effect on the time to emitter localisation. In the subsequent section, the path planning algorithms applied to quantify this effect are presented.

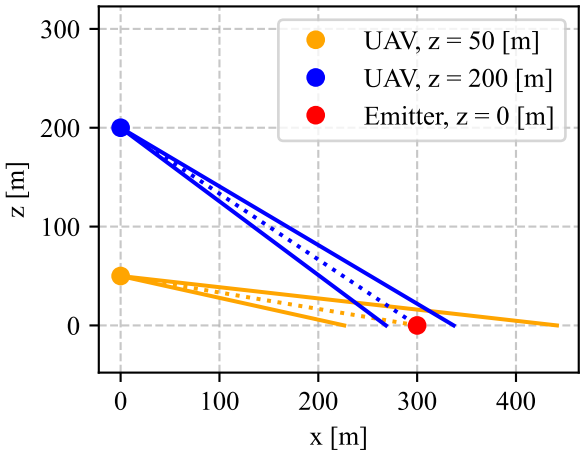

Fig. 2: The RF direction-finding antenna mounted on the respective UAV (blue/orange) acquires the bearing to the ground-level emitter (red, z = 0 [m]). Extending the true radar line of sight (dotted blue/orange line) by the assumed standard deviation of 3° (solid blue/orange line), results in the probable area where the emitter location is expected. Measurements from a higher altitude (blue UAV, z = 200 [m]) result in a smaller cross-sectional area at ground level compared to those from a lower altitude (orange UAV, z = 50 [m]).

III. Control Algorithms

The evaluation in this paper is focused on the effect of variable altitude control on the FIM controller. The FIM controller utilizes the Fisher information of the current belief state to steer the platform into the position of maximal information gain. To benchmark the FIM controller the *Loitering* controller is also introduced.

A. FIM Controller

The principle behind the FIM controller was applied by [14] with the additional restriction to a fixed flight altitude. [14] computes the desired setpoint from a policy which incorporates the covariance matrix of the current belief and the Fisher information matrix. In the following section the

statistical equations required to employ the FIM controller are described. As the measurements are corrupted by Gaussian noise, only an estimate of the emitter location can be produced. Since the emitter is assumed to be stationary, no emitter dynamics must be considered by the estimator. Additionally due to the invoked nonlinearities of the emitter state a Kalman Filter would poorly assume the posterior to be Gaussian. As the alternative to the Kalman Filter for this case a grid-based Bayes filter is applied.

1) Grid-Based Bayes Filter: The grid in this paper is discretized by 350x350 grid points in the *xy*-plane. In principle a measurement results in a belief over the current emitter state, which contributes via Bayes' theorem to the posterior belief of the emitter state. The emitter location is estimated from the maximum a posteriori probability

$$\hat{\mathbf{x}}_{e,k} = \check{\mathbf{x}}_{k,i^*j^*}\,, \tag{6}$$

with

$$(i^*, j^*) = \underset{i,j\,\in\, I}{\operatorname{argmax}}\, p_{k,ij}\,, \tag{7}$$

and $p_{k,ij}$ being the values from the posterior probability density at each grid point i, j out of the set of all grid point indices $I = \{1, ..., X^b\} \times \{1, ..., Y^b\}$.

The estimated covariance matrix $\hat{\mathbf{P}}_{e,k}$ of the posterior probability distribution $p_{k,ij}$ is computed by

$$\hat{\mathbf{P}}_{e,k} = \sum_{i=1}^{X^b}\sum_{j=1}^{Y^b} p_{k,ij}\Delta x^b \Delta y^b (\check{\mathbf{x}}_{k,ij} - \hat{\mathbf{x}}_{e,k})(\check{\mathbf{x}}_{k,ij} - \hat{\mathbf{x}}_{e,k})^T \tag{8}$$

with $\hat{\mathbf{x}}_{e,k}$ centering the covariance matrix at the estimate emitter coordinate and $\check{\mathbf{x}}_{k,ij}$ denoting the center of the respective grid point. Δx^b and Δy^b denote the edge length of a square covering the area of a single grid point. The superscript b relates the respective variables to the belief grid.

2) Fisher Information Matrix: The available information in a measurement can be quantified with the help of the (FIM) [4]–[6]. The FIM of the current measurement can be written as

$$\mathbf{J} = \mathbf{H}_k^T \mathbf{R}_k^{-1} \mathbf{H}_k \tag{9}$$

with $\mathbf{R}$ as defined in (5) and $\mathbf{H}$ being the Jacobian of the measurement function $\mathbf{z}$

$$\mathbf{H} = \begin{bmatrix} \frac{\partial h_{az}}{\partial \Delta x} & \frac{\partial h_{az}}{\partial \Delta y} \\ \frac{\partial h_{el}}{\partial \Delta x} & \frac{\partial h_{el}}{\partial \Delta y} \end{bmatrix} \tag{10}$$

$$= \begin{bmatrix} \frac{\Delta y}{\Delta x^2 + \Delta y^2} & -\frac{\Delta y}{\Delta x^2 + \Delta y^2} \\ \frac{-\Delta x \Delta z}{r^2\sqrt{\Delta x^2 + \Delta y^2}} & \frac{-\Delta y \Delta z}{r^2\sqrt{\Delta x^2 + \Delta y^2}} \end{bmatrix} \tag{11}$$

$$= \begin{bmatrix} a & b \\ c & d \end{bmatrix}. \tag{12}$$

The partial derivatives $\frac{\partial h_{az}}{\partial \Delta x}$ and $\frac{\partial h_{az}}{\partial \Delta y}$ of the azimuth measurement are independent of the z coordinate and only dependent on the maneuver in xy-plane. Combining (5) and (III-A2) into (9) results in

$$\mathbf{J} = \begin{bmatrix} \frac{a^2}{(\sigma_{az})^2} + \frac{c^2}{(\sigma_{el})^2} & \frac{ab}{(\sigma_{az})^2} + \frac{cd}{(\sigma_{el})^2} \\ \frac{ba}{(\sigma_{az})^2} + \frac{dc}{(\sigma_{el})^2} & \frac{b^2}{(\sigma_{az})^2} + \frac{d^2}{(\sigma_{el})^2} \end{bmatrix}. \tag{13}$$

3) Determination of the Control Input: Based on [14] and [5] an optimization problem is derived to select the optimal control input

$$\min_{\mathbf{u}_{k+1}} \quad \pi \cdot \sqrt{\det\left((\hat{\mathbf{P}}_{e,k})^{-1} + \mathbf{J}_{k+1}\right)^{-1}} \tag{14}$$

$$\text{s. t.} \quad ||\mathbf{u}_{k+1}||_2 \quad \leq \quad r_{bound}\,, \tag{15}$$

with $\mathbf{u}_{k+1}$ as the control action, the current estimated covariance $\hat{\mathbf{P}}_{e,k}$ and $\mathbf{J}_{k+1} = J(\mathbf{u}_{k+1})$. The maximization of $\mathbf{u}_{k+1}$ leads by eq. 3 to $\mathbf{x}_p$ that results in the maximal information gain over the emitter position estimate $\hat{\mathbf{x}}_{e,k}$. $\mathbf{u}_{k+1}$ is searched within the action space constrained by the radius r_{bound}. 14 is derived from the formula for the area $\mathbf{A}$ of the uncertainty region

$$\mathbf{A} = \pi \cdot \sqrt{\det\left((\hat{\mathbf{P}}_{e,k})^{-1}\right)}\,. \tag{16}$$

$(\hat{\mathbf{P}}_{e,k})^{-1}$ can be substituted with $\mathbf{J}_k$ to result in the area $\mathbf{A}$ of the 1σ Cramer Rao lower bound ellipsoid.

If the sensor platform's movement is constrained by a maximal velocity v_{max}, the actual applied control input may be different from $\mathbf{u}_{k+1}$. In the case of $r_{bound} > ||\mathbf{x}_p - \mathbf{x}_e||_2$ the optimization problem finds $\mathbf{u}_{k+1}$ to steer to the optimum within the whole observed space, which is in close proximity of $\mathbf{x}_e$. If $r_{bound}/\Delta T > v_{max}$ the desired setpoint is not reachable and only the direction of $\mathbf{u}_{k+1}$ is realized. For the myopic application of the optimizer in this paper we set $r_{bound}/\Delta T = v_{max}$.

The termination criterion of the emitter localization algorithm is the inequality

$$\lambda_1(\hat{\mathbf{P}}_{e,k}) + \lambda_2(\hat{\mathbf{P}}_{e,k}) \quad \leq \quad 10[m]\,. \tag{17}$$

If the sum of the estimated covariance matrix eigenvalues $\lambda_i(\hat{\mathbf{P}}_{e,k})$ is lower than 10 [m], the simulation loop terminates with termination time $t_{term} = t_k$ and assumes the emitter position to be accurately estimated. In the computation of $\hat{\mathbf{P}}_{e,k}$, the ratio between the number of grid points and the total covered grid area is considered in order to set the unit in eq. 17 to *meters*.

B. Loitering controller

To benchmark the control algorithms, a control approach from [13] is utilized. The *Loitering* controller steers the platform in a circular motion around the estimated emitter position. The controller follows the circle that is spanned

around the estimated emitter position while maintaining the current distance between the emitter and the platform. This is done by rotating the platforms direction of flight yaw angle to an offset of az_{sp} = 90° to the azimuth bearing angle. The controller was adapted to also control the platforms altitude to steer the measurement elevation angle to el_{sp} = 45°.

IV. Scenarios

All scenarios consist of one sensor platform and one stationary emitter. The sensor platform is initialized at the altitude $z_{t=0}$, while the emitter is assumed to be at ground level z = 0. The initial position of the sensor platform is taken from the sets

$$x_{p,t=0}[m] \in \{300, 400, 700, 1100, 1700, 2600, 3900\} \quad (18)$$

$$z_{t=0}[m] \in \{10, 25, 50, 100, 200\}, \quad (19)$$

with $y_{p,t=0} = x_{p,t=0}$. This initialization results in the set of initial distances $d_{xy,t=0} = \sqrt{{x_p}^2 + {y_p}^2}$

$$d_{xy,t=0}[m] \in \{424, 566, 990, 1556, 2404, 3677, 5515\}. \quad (20)$$

The emitter ground truth for all scenarios is at $\mathbf{x}_e = [0, 0, 0]^T\ [m]$. The covariances on the bearing measurements are assumed to have a greater uncertainty on the elevation measurement and thus are set to σ_{az} = 3 and σ_{el} = 6. The applied controller are selected from controller-type $c \in \{FIM, \textit{Loitering}\}$. Both controller are simulated with the ability to control the flight altitude $\in \{\textit{fixed}, \textit{variable}\}$.

All control inputs and sensor computations are discretized on ΔT = 1 [s] and r_{bound} is set to 10 [m]. The parameter r_bound results from the maximum platfrom speed $v_{p,max} = 10\,m/s$. The platform underlies further no acceleration or deacceleration restrictions.

To quantify the difference between t_{term} of different controller, the relative termination time

$$t_{term,rel}(c_1, c_2) = \frac{t_{term,c_1} - t_{term,c2}}{t_{term,c1}} \quad (21)$$

is introduced, depending on the controller type c_1 and c_2 applied in the considered comparison.

V. Simulation Results

The simulations are conducted in Python 3.11 and written in the framework of the Python package gym 0.28.1 from OpenAI [15]. The optimization problem is solved by the numeric solver IPOPT and the framework CASADI in Python 3.11.

The simulation results of the *FIM* controller and the *Loitering* controller each with altitude control *fixed* and *variable* are evaluated. All simulations are done with the parameters from set described in IV. The emitter position and the covariance matrix are estimated with the grid-based Bayes filter described in III-A1.

A. Single Scenario Evaluation

Figure 3 shows the flight paths of the different control algorithms are applied to a single scenario featuring the same initial sensor platform and emitter coordinates.

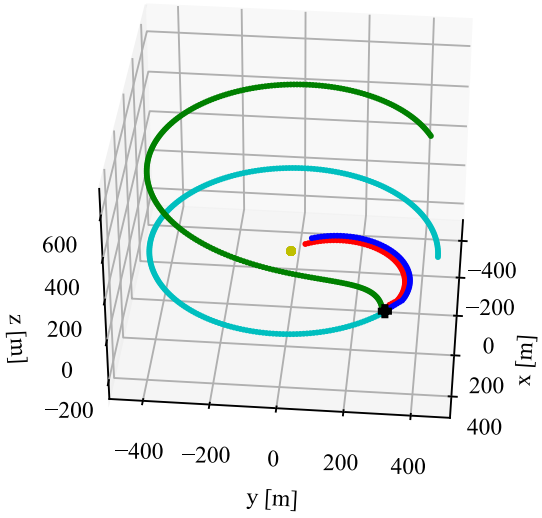

(a)

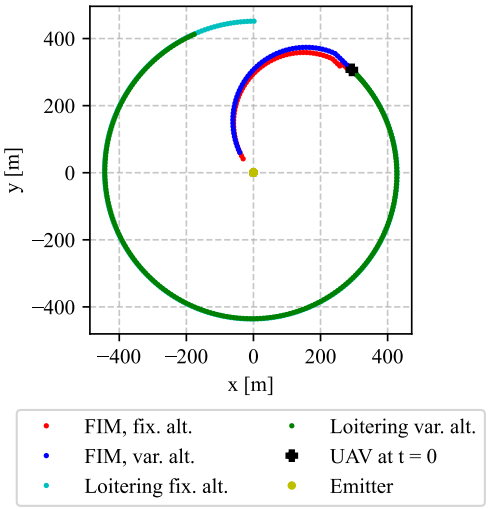

(b)

Fig. 3: Resulting flight paths of the sensor platform starting at the initial position marked with the cross, in 3a in xyz and in 3b in xy-plane. The different paths result from the different control approaches FIM controller with *fixed* altitude control (red), FIM Controller with altitude control *variable* (dark blue), loitering-controller with *fixed* altitude control (light blue), *loitering* controller with *variable* altitude control (green). The paths have different lengths as the termination criterion is reached at different times t_{term}.

In the scenario shown in figure 3 both *FIM* controller reach t_{term} earlier than the *Loitering* controller. The flight path of the FIM controller in this scenario gathers the information over the emitter state more efficiently resulting in a lower t_{term}. The exact values of the scenario shown in figure 3 are summarized in table I.

TABLE I: Termination Time t_{term}

	FIM		*Loitering*	
	var. alt	fix. alt.	var. alt	fix. alt
t_{term} [s]	60	63	234	241

Changing the altitude control setting only slightly alters the xy-plane path of both controller. The *FIM* controller simultaneously circles the emitter and closes the distance to the emitter. The controller with *variable* altitude enabled maneuver a major part of their altitude change at the beginning of the flight. The path taken by the *Loitering* controller differs vastly from the path of the *FIM* controller, as the controller steers to maintain a constant radius to the emitter.

B. Influence of Elevation Standard Deviation

The influence of the measurement standard deviation σ_{el} and σ_{az} of the angle measurements is also evaluated with different scenario simulations. While keeping σ_{az} fixed at 3°, σ_{el} is varied $\in \{3, 6, 9\}$.

The results of a single scenario run with varied σ_{el} are summarized in table II.

TABLE II: Influence of σ_{el} on t_{term}

	$t_{term}[s]$	
σ_{el}	FIM, var. alt.	FIM, fix. alt.
3°	53	61
6°	60	63
9°	63	64

Table II shows a decreasing t_{term} for decreasing σ_{el} and as expected, the lowest t_{term} results from the scenario with the lowest simulated σ_{el} = 3°. In the case of the *FIM* controller with *variable* altitude the improvement of decreasing σ_{el} is significantly greater than for the case of *fixed* altitude. For all remaining scenarios the measurement covariances are fixed at σ_{el} = 6° and σ_{az} = 3°. The advantage of the *variable* altitude controller over the *fixed* altitude controller becomes negligible for higher values of σ_{el}. As shown in figure 2 $z_{t=0}$ has a great influence on the size of the expected area. However, in the case of σ_{el} = 9° the maneuver towards the emitter in *xy*-plane yields greater information gain than the change of altitude. This leads to diminishing time advantage of the *variable* altitude controlled scenarios.

C. Evaluation of all Scenarios

The focus in this section is on evaluating the controller behavior over the complete set of scenarios defined in IV. The evaluation starts with a comparison of the complete set of scenarios, before the influences of individual scenario parameter such as $d_{xy,t=0}$ and $z_{t=0}$ are evaluated.

The overall result of the scenarios can be found in table III. Here the average termination time $\bar{t}_{term}$ of all recorded scenarios is summarized for both control approaches *FIM* and *Loitering*, each with *variable* and *fixed* altitude.

TABLE III: Mean Termination Time $\bar{t}_{term}$

	FIM		*Loitering*	
	var. alt	fix. alt.	var. alt	fix. alt
$\bar{t}_{term}$	315	338	570	618

Over all simulations the *FIM* controller with *varying* altitude localized the emitter after 315 [s]. The *FIM* controller with *fixed* altitude performed worse with a mean value of 338 [s]. The *Loitering* controller took 570 [s] with *variable* altitude control enabled and 618 [s] without, to localize the emitter. The $\bar{t}_{term}$ over all scenarios shows a 7% improvement for enabling *variable* altitude control in the *FIM* controller. Comparing the $\bar{t}_{term}$ of the *variable* altitude *FIM* controller with the *Loitering* controller with *variable* an improvement of 45% is observed. Compared to the *fixed* altitude $Loitering$ controller an improvement of 49% is achieved by the *FIM variable* altitude controller. As expected, the *FIM* controller with *variable* altitude shows the lowest $\bar{t}_{term}$.

The above results showed the general behavior of the different controller and the influence of the controller settings. The controller utilizing the Fisher information with enabled *variable* altitude control performed as expected with the lowest t_{term}. Interestingly the gap between the fixed and variable altitude *FIM* controller is not as far as expected. Thus, in the following the investigation of the effect on the time efficiency regarding *variable* altitude control is focused on the simulation results of the *FIM* controller. The first evaluation focuses on the the course of t_{term} for scenarios only varying $d_{xy,t=0}$, then the evaluation focuses on scenarios only varying $z_{t=0}$.

1) Scenarios with varying initial distance in xy-plane $d_{xy,t=0}$: In figure 4 the dependency of t_{term} over varying $d_{xy,t=0}$ is evaluated. The $\bar{t}_{term,rel}$ is computed from the relative difference of the termination times average over all $z_{t=0}$ between the *variable* and the *fixed* altitude *FIM* controller. $\bar{t}_{term,rel}$ and $\bar{t}_{term}$ of the considered scenarios are shown in figure 4b. For improved readability of $\bar{t}_{term}$ in 4a only scenarios with $z_{t=0} = 200\,[\mathrm{m}]$ are considered.

The evaluation of the scenarios in figure 4a show a persisting gap between the altitude control modes over the varying $d_{xy,t=0}$. The same behavior as presented in figure 4a was observed for all other $z_{t=0}\,[\mathrm{m}]$ out of the simulated scenarios. The difference between t_{term} of the different altitude control modes of the *FIM* controller is staying close to the range between 5% and 10%. Focusing the evaluation on the considered $d_{xy,t=0}$ does not reveal any explicit dependency towards t_{term}.

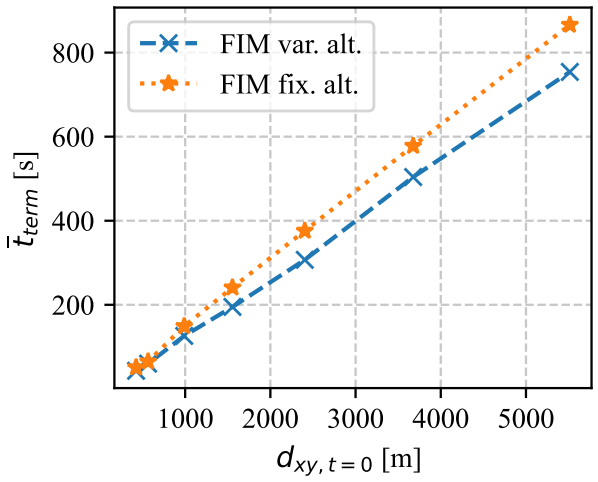

(a)

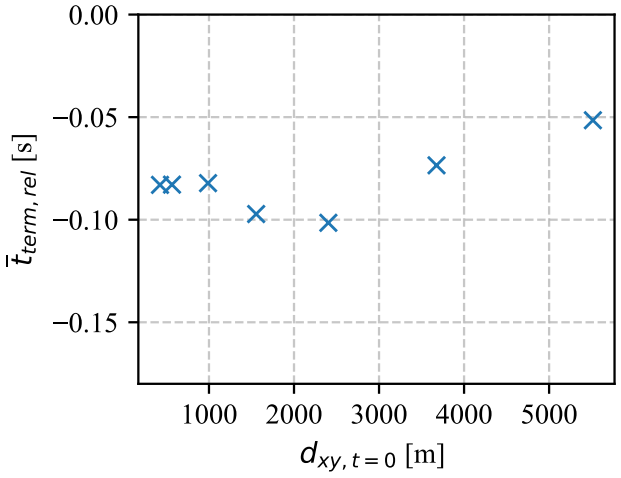

(b)

Fig. 4: 4a describes t_{term} of the *FIM* controller with *variable* and *fixed* altitude control over varying $d_{xy,t=0}$. Only scenarios with $z_{t=0} = 200$ [m] are shown in 4a for improved readability. 4b describes the resulting $\bar{t}_{term,rel}$ as average over all $z_{t=0}$ depending on varying $d_{xy,t=0}$.

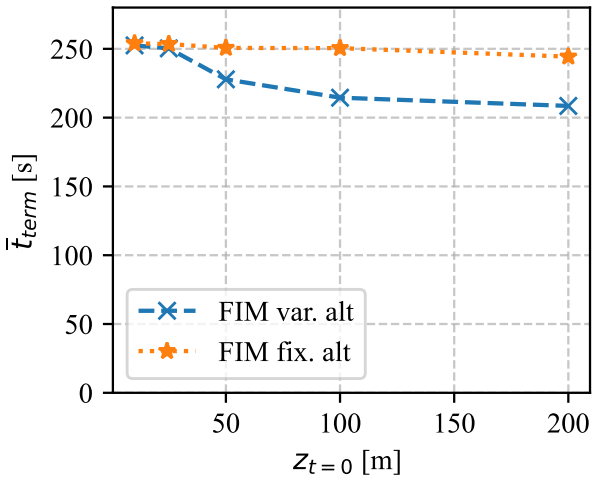

(a)

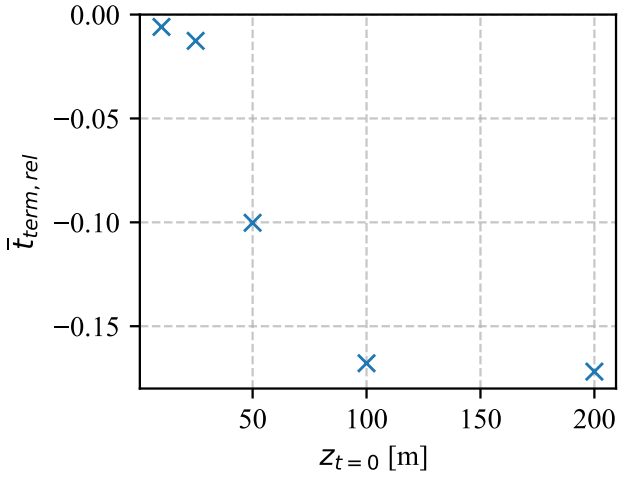

(b)

Fig. 5: Total termination time $\bar{t}_{term}$ 5a and relative difference of termination time $\bar{t}_{term,rel}$ 5b of the *FIM* controller with *variable* and *fixed* altitude control over the $z_{t=0}$. The mean values are computed over all considered $d_{xy,t=0}$.

2) Scenarios with varying initial altitude $z_{t=0}$: The following evaluations involve varying $z_{t=0}$ to explore a potential dependency between t_{term} and $z_{t=0}$. The comparison of the total $\bar{t}_{term}$ and the relative $\bar{t}_{term,rel}$ between the *variable* and *fixed* altitude controller is shown in figure 5. The average values $\bar{t}_{term}$ and $\bar{t}_{term,rel}$ considered here are the averages over all $d_{xy,t=0}$.

$\bar{t}_{term}$ decreases slightly for increasing $z_{t=0}$ in the case of the *fixed* altitude *FIM* controller. The *variable* altitude *FIM* controller on the other hand improves its efficiency with increasing $z_{t=0}$. The difference between the altitude control settings with varying $z_{t=0}$ is highlighted by $\bar{t}_{term,rel}$. $z_{t=0}$ has a high influence of up to 17% on the termination times at $z_{t=0} \in \{200, 100\}$. For $z_{t=0} = 50$ [m] the influence on $\bar{t}_{term}$ is 10 %. For values of $z_{t=0} = 10$ [m] and $z_{t=0} = 25$ [m], the $\bar{t}_{term,rel}$ between the scenarios with variable and *fixed* altitude control becomes less than 2%. This behavior is explained by the similar paths the different altitude control modes take as shown in figure 3b.

VI. Conclusion and Future Work

Out of the compared controller the *FIM* controller with *variable* altitude control performs best regarding the time until successful emitter localization as expected. The improvements towards the benchmark controller regarding the $\bar{t}_{term}$

is 49%. As expected, the application of the *FIM* controller with *variable* altitude control also improves compared to the *fixed* altitude controller. However, the relative improvement of 7% lower $\bar{t}_{term}$ was not as significant as expected. The evaluations showed that for $z_{t=0} < 50$ [m] the FIM with *variable* altitude control follows a path close to the path of the FIM with *fixed* altitude control. Only for $z_{t=0} > 50$ [m] an improvement of greater than 10% $\bar{t}_{term,rel}$ was observed. The evaluation showed a significant influence of σ_{el} on the localization efficiency for the case of *variable* altitude control. Increasing σ_{el} to value of 9° almost completely negates the advantage of the *variable* altitude control.

The exact reason why the $\bar{t}_{term,rel}$ drops as significant as observed for $z_{t=0} > 50$ [m] may require further investigation of the gradient of the objective function values. Also an evaluation of the radius in which the optimal action is searched for may yield valuable insight regarding this behaviour. For further investigations on the effect of *variable* altitude control alternatives to the *FIM* controller may be evaluated. The exploration of different control strategies may result in improvements for the scenarios in which the *FIM* controller performs less efficient.

To determine whether the effort of enabling variable altitude flight is justified by the resulting efficiency gains, a thorough evaluation of the available hardware and the knowledge about the specific application scenario needs to be conducted for each real-world scenario individually. In the case of an application in which the localization is started at $z_{t=0} < 50$ [m] the time efficiency gain does not outweigh the required hardware and software adaptions to enable *variable* altitude control.

REFERENCES

[1] H. V. Nguyen, F. Chen, J. Chesser, H. Rezatofighi, and D. Ranasinghe, "LAVAPilot: Lightweight uav trajectory planner with situational awareness for embedded autonomy to track and locate radio-tags," *IEEE International Conference on Intelligent Robots and Systems*, pp. 2488–2495, oct 2020.

[2] C. Leung, S. Huang, N. Kwok, and G. Dissanayake, "Planning under uncertainty using model predictive control for information gathering," *Robotics and Autonomous Systems*, vol. 54, no. 11, pp. 898–910, nov 2006.

[3] F. Hoffmann, A. Charlish, M. Ritchie, and H. Griffiths, "Sensor path planning using reinforcement learning," *Proceedings of 2020 23rd International Conference on Information Fusion, FUSION 2020*, jul 2020.

[4] J. P. Le Cadre and H. Gauvrit, "Optimization of the observer motion for bearings-only target motion analysis," *ADFS 1996 - Australian Data Fusion Symposium*, pp. 190–195, 1996.

[5] Y. Oshman and P. Davidson, "Optimization of observer trajectories for bearings-only target localization," *IEEE Transactions on Aerospace and Electronic Systems*, vol. 35, no. 3, pp. 892–902, 1999.

[6] M. L. Hernandez, "Optimal sensor trajectories in bearings-only tracking," *Proceedings of the Seventh International Conference on Information Fusion, FUSION 2004*, vol. 2, no. January 2004, pp. 893–900, 2004.

[7] S. M. Dehghan, H. Moradi, and S. A. Shahidian, "Optimal path planning for DRSSI based localization of an RF source by multiple UAVs," *2014 2nd RSI/ISM International Conference on Robotics and Mechatronics, ICRoM 2014*, pp. 558–563, dec 2014.

[8] O. M. Cliff, R. Fitch, S. Sukkarieh, D. L. Saunders, and R. Heinsohn, "Online localization of radio-tagged wildlife with an autonomous aerial robot system," *Robotics: Science and Systems*, vol. 11, 2015.

[9] F. Hoffmann, A. Charlish, M. Ritchie, and H. Griffiths, "Policy Rollout Action Selection in Continuous Domains for Sensor Path Planning," *IEEE Transactions on Aerospace and Electronic Systems*, vol. 57, no. 4, pp. 2247–2264, 2021.

[10] S. S. Ponda, R. M. Kolacinski, and E. Frazzoli, "Trajectory optimization for target localization using small unmanned aerial vehicles," *AIAA Guidance, Navigation, and Control Conference and Exhibit*, 2009. [Online]. Available: https://arc.aiaa.org/doi/10.2514/6.2009-6015

[11] DJI, "Matrice 600 User Manual," pp. 1–72, 2016. [Online]. Available: http://www.dji.com/product/matrice600/info#downloads

[12] S. Venkateswaran, J. T. Isaacs, K. Fregene, R. Ratmansky, B. M. Sadler, J. P. Hespanha, and U. Madhow, "RF source-seeking by a micro aerial vehicle using rotation-based angle of arrival estimates," *Proceedings of the American Control Conference*, pp. 2581–2587, jun 2013.

[13] I. H. Wang, V. N. Dobrokhodov, I. I. Kaminer, and K. D. Jones, "On vision-based target tracking and range estimation for small UAVs," *Collection of Technical Papers - AIAA Guidance, Navigation, and Control Conference*, vol. 7, pp. 5507–5517, 2005.

[14] F. Hoffmann, "Sensor Path Planning for Emitter Localization," Ph.D. dissertation, 2023.

[15] J. U. Towers, Mark and Terry, Jordan K. and Kwiatkowski, Ariel and Balis, "Gymnasium." [Online]. Available: https://zenodo.org/record/8127025